

# Electronic Fingerprint of the Protonated Imidazole Dimer Probed by X-ray Absorption Spectroscopy

Sambit K. Das,<sup>\*,§</sup> Marc-Oliver Winghart,<sup>\*,§</sup> Peng Han, Debkumar Rana, Zhuang-Yan Zhang, Sebastian Eckert, Mattis Fondell, Thomas Schnappinger, Erik T. J. Nibbering,<sup>\*</sup> and Michael Odelius<sup>\*</sup>



Cite This: *J. Phys. Chem. Lett.* 2024, 15, 1264–1272



Read Online

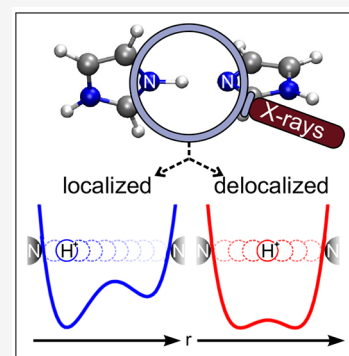
ACCESS |

Metrics & More

Article Recommendations

Supporting Information

**ABSTRACT:** Protons in low-barrier superstrong hydrogen bonds are typically delocalized between two electronegative atoms. Conventional methods to characterize such superstrong hydrogen bonds are vibrational spectroscopy and diffraction techniques. We introduce soft X-ray spectroscopy to uncover the electronic fingerprints for proton sharing in the protonated imidazole dimer, a prototypical building block enabling effective proton transport in biology and high-temperature fuel cells. Using nitrogen core excitations as a sensitive probe for the protonation status, we identify the X-ray signature of a shared proton in the solvated imidazole dimer in a combined experimental and theoretical approach. The degree of proton sharing is examined as a function of structural variations that modify the shape of the low-barrier potential in the superstrong hydrogen bond. We conclude by showing how the sensitivity to the quantum distribution of proton motion in the double-well potential is reflected in the spectral signature of the shared proton.



Low-barrier hydrogen bonds (LBHBs) constitute a special type of chemical bond where the  $pK_a$  of the two heteroatoms are closely matched, allowing the hydrogen to be more equally shared.<sup>1–3</sup> Especially short superstrong hydrogen bonds result in a heavy atom distance of  $<2.55$  Å.<sup>2,4,5</sup> LBHBs are understood to occur under particular circumstances, enhancing enzymatic catalysis,<sup>6,7</sup> or in proton transport in hydrogen fuel cells.<sup>8–10</sup> Until now, major methods for the characterization of LBHBs comprised vibrational spectroscopy, diffraction techniques, and quantum chemistry calculations. The most important conclusion drawn from these studies is that there is a major change in the charge distribution around the shared hydrogen atom and the electronegative atoms forming the superstrong hydrogen bond. There is a clear increase in the covalent over the electrostatic contributions compared to those of common hydrogen bonds (known as “weak” hydrogen bonds) such as in water. Superstrong hydrogen bonds are different with respect to the potential well of the hydrogen stretching mode: as opposed to an anharmonic (Morse-type) single-well potential, the nature and dynamics of shared protons are characterized by a double-well potential, which may be symmetric or asymmetric. The central barrier accompanying such a double-minimum potential is in many cases so low that the  $\nu = 0$  state lies above the barrier, with distinctive consequences for the vibrational signatures<sup>5,11,12</sup> and the location of the proton (the  $\nu = 0$  wave function has its maximum halfway between the two electronegative atoms). Shared proton complexes are a subgroup of LBHBs, where the net charge of the two units forming the superstrong hydrogen bond is positive. The majority of the

work on shared proton studies has focused on the hydrated proton complexes.<sup>12,13</sup> In particular, there is major relevance of these shared proton motifs within the context of proton transport (von Grothuss mechanism) where Zundel and Eigen motifs are considered to be key structural configurations.<sup>11,14</sup> Insights into the dynamics of proton exchange have been obtained from nuclear magnetic resonance (NMR),<sup>15</sup> revealing that the average proton hopping time in water is 1 ps, and from ultrafast infrared (IR) spectroscopy, which has allowed sequential steps and corresponding time scales as well as possible geometrical configuration involved in this process to be deciphered.<sup>16–18</sup> Ab initio molecular dynamics (AIMD) simulations have shown an interconversion between Eigen (hydronium)-like geometries and Zundel-like geometries, with the major impact on hydrogen bond rearrangements of the hydration shells.<sup>19–21</sup> Fluctuations in the surrounding hydrogen bond network strongly influence LBHBs and effectuate proton transfer in aqueous solution.<sup>19,22–25</sup>

The electronic structural properties of shared proton motifs have been less explored. In recent years, soft X-ray spectroscopy has emerged as an effective technique in this field, which, thanks to its element specificity, enables targeted probing of

**Received:** December 21, 2023

**Revised:** January 19, 2024

**Accepted:** January 23, 2024

**Published:** January 26, 2024



the heteroatoms engaged in hydrogen bonding.<sup>26–28</sup> In particular, we have investigated the hydrated proton complex in acetonitrile solution and concluded that orbital interactions of the water molecules directly hydrating the proton change significantly compared to those of water (as a monomer in acetonitrile solution or as part of an aqueous solution).<sup>29</sup>

In this letter, we aim to elucidate the fundamental steps behind the excellent proton conductivity of imidazole, a molecule that, just like water, is amphoteric and can mediate proton transport in a similar sequential von Grothuss-type fashion.<sup>30–34</sup> Technical applications such as high-temperature proton exchange membrane fuel cells,<sup>35</sup> enzymatic catalysis,<sup>36–38</sup> and biological signal transduction<sup>39</sup> rely on the special hydrogen bonding capabilities of imidazole for their functionality.

Imidazoles and their hydrogen bonding interactions have been the subjects of previous X-ray spectroscopic studies<sup>40–42</sup> utilizing the high sensitivity of core-level spectroscopy to the local chemical and structural environment. Two well-separated N K-edge resonances were observed due to the promotion of an  $N_{1s}$  core electron either from the N–H side or from the N lone-pair side of the imidazole molecule into the unoccupied  $\pi^*$  orbital. Both of these pre-edge transitions were also found to undergo chemical shifts when comparing isolated imidazole in the gas phase to the crystalline or solution phase, which can be attributed to the formation of intermolecular hydrogen bonds between the imidazole moieties and/or with solvent molecules.<sup>41</sup>

Here we demonstrate a joint experimental and theoretical investigation of the solvated protonated imidazole dimer, which represents the quintessential subunit of proton-conducting imidazole chains. Under conditions where two imidazole molecules have to accommodate a shared excess proton, we scrutinize the formation of an LBHB and characterize the associated double-well potential between the two imidazole moieties. Starting with an IR spectroscopic analysis where the peculiarities of various shared proton species have already been benchmarked, we continue with nitrogen K-edge absorption spectroscopy and aim at identifying the electronic fingerprint of the protonated dimer. With the help of theory, we address the question as to how the degree of localization of the proton and thus the barrier height and the symmetry of the potential are imprinted into the X-ray signatures. To this end, we have explored the influence of structural changes in the geometry of the dimers as well as the role of the solvation shell and discuss the two limiting cases of a rather localized proton and a quasi-barrier-free shared proton. As a result, we are able to draw a conclusion on the sensitivity of the X-ray probe as a novel method for characterizing shared proton motifs and outline the implications for possible future studies. Complementary experimental and computational data are presented in Figures S1–S12 and Tables S1–S3 in the Supporting Information.

Figure 1 shows the IR absorption spectra of imidazole, imidazolium, and a mixture of both in ethanol at multimolar concentrations, providing the first insight into the effect of excess protons on imidazole-containing solutions and allowing conclusions to be drawn about the chemical speciation. The spectra of pure HIm and HImH<sup>+</sup> consist of molecular vibrations in the fingerprint region below 1700  $\text{cm}^{-1}$  and a broader progression of peaks from the N–H stretching region from 3200 to 2500  $\text{cm}^{-1}$ . In comparison, the spectrum containing a 1:1 mixture of HIm and HImH<sup>+</sup> (i.e., with a

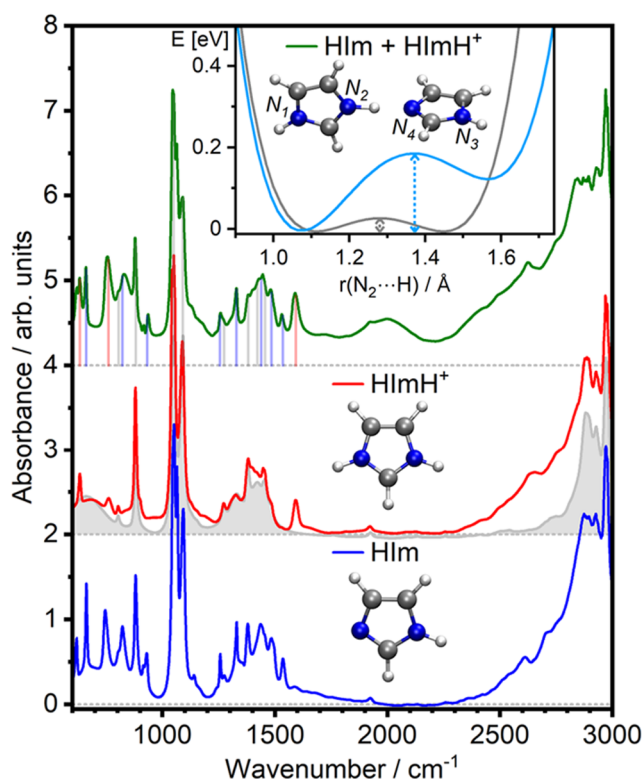


**Figure 1.** FTIR spectra of a mixture of imidazole with imidazolium bromide (green;  $c = 6$  M each), pure imidazolium iodide (red;  $c = 2.5$  M), and imidazole (blue;  $c = 6$  M) in ethanol (light gray). Colored bars indicate energy transitions of the pure compounds. Inset: ground-state potential energy surface along the proton displacement coordinate of the solvated HIm-H<sup>+</sup>-ImH dimer in its asymmetric (blue) and symmetric (gray) geometries.

nominal excess of half a proton per imidazole molecule) exhibits a peak at 2050  $\text{cm}^{-1}$  and a broadband offset over the entire range of the spectrum from 600 to 3000  $\text{cm}^{-1}$ , not observable in the spectra of the pure compounds. Similarly broad absorption bands were previously observed for protons solvated by H<sub>2</sub>O and attributed to the proton-transfer mode in Zundel motifs and to combination modes and overtones of the proton-transfer mode.<sup>43</sup> This so-called Zundel continuum was attributed to the presence of a characteristic double-minimum potential along the proton-transfer coordinate of the Zundel cation, which is highly sensitive to fluctuating local electric fields caused by the rapidly moving solvent environment.<sup>16</sup> Accordingly, we interpret the appearance of a broad absorption continuum in the IR spectra of the imidazole/imidazolium mixture as indicative of a superstrong Zundel-like hydrogen bond between neighboring imidazole molecules sharing an excess proton, namely, the HIm-H<sup>+</sup>-ImH dimer.

To corroborate this initial assumption, we performed DFT calculations on the ground-state potential energy surface (PES) of the HIm-H<sup>+</sup>-ImH dimer in which we account for the solvent environment using a polarizable continuum model and explicit solvation of the outer N–H groups. (See Figure S5 for a full overview of the calculated structures, optimized in the Gaussian 16 software package.<sup>44–46</sup>) Similar to a previous study of the isolated dimer,<sup>47</sup> we find a global minimum structure in which the planes of the heteroaromatic rings are rotated by 90.6° with respect to each other and where the central proton is found to be significantly closer to one side of

the dimer with a N–H bond length of 1.097 Å. This results in two unequal rings, one of which has more imidazolium-like character and the other that has an imidazole-like structure (Figure S6). As a consequence, a rigid scan of the PES along the N⋯H⋯N coordinate with the dimer frozen in its global minimum geometry yields an asymmetric double-well potential shown in the inset of Figure 1. Notably, we obtain a barrier height of 0.17 eV ( $\sim 1400\text{ cm}^{-1}$ ) from the optimized minimum which is above the harmonic zero-point energy (ZPE) of 0.13 eV of the N–H stretch normal mode ( $\nu = 2160.54\text{ cm}^{-1}$ ). This suggests a higher degree of localization of the excess proton on one side of the dimer. In contrast, the geometrically relaxed saddle point, where the shared proton is in the middle of the dimer, yields a much reduced barrier height of 0.04 eV (i.e., well below the ZPE). The latter finding coincides qualitatively with earlier gas-phase studies<sup>47–49</sup> and, with its more delocalized description of the shared proton, is in line with the experimentally observed broad Zundel-like IR absorption bands. Since the rigid scans are restricted to changing only one parameter, the N–H distance, it is important to point out the intrinsic multidimensionality of the system: additional degrees of freedom of the imidazole moieties as well as fluctuations in the solvation shell are known to influence the potential energy landscape, experienced by the shared proton,<sup>16</sup> and thus would require the sampling of a whole range of structures via AIMD simulations. However, as this is beyond the scope of this study, we focus on the description of the asymmetric and symmetric model potentials, which we also refer to as *Asymm<sup>solv</sup>* and *FlatSymm* (Figure S5). In doing so, we take into account the particularly important coordinate of the central N⋯N distance, which shrinks from 2.660 to 2.561 Å from the asymmetric to the symmetric structure. From the Zundel water model, it is known that the shape of the potential along the proton displacement coordinate is strongly dependent on the separation between the hydrogen bonding atoms, effectively modulating the barrier height.<sup>19</sup> In this respect, the two presented structures are to be considered as limiting cases and form the starting point for the ensuing discussion of the experimental X-ray results.

Utilizing the capability of soft X-ray spectroscopy to report on the protonation state of molecules from an electronic structural point of view,<sup>50,51</sup> we have explored the impact of sharing a proton in the HIm–H<sup>+</sup>–ImH complex on the nitrogen core excitations. As depicted in Figure 2a, nitrogen K-edge absorption spectra of imidazole, imidazolium, and their 1:1 mixture in ethanol were measured in transmission mode using a liquid flatjet setup at the BESSY II synchrotron.<sup>52–54</sup> Note that the background of nonresonant contributions from the solvent, counterions, and imidazole atoms other than nitrogen was subtracted in a least-squares fitting routine based on tabulated atomic absorption cross sections.<sup>55</sup> In good agreement with a previous study performed in H<sub>2</sub>O in total fluorescence yield mode,<sup>42</sup> our measurements reveal X-ray absorption bands at 400.1 and 401.7 eV for HIm and at 401.5 eV for HImH<sup>+</sup>. Owing to the two chemically different nitrogen sites (N–H and N lone pair), these transitions with  $N_{1s} \rightarrow \pi^*$  character split into two peaks 1.6 eV apart for HIm, while the symmetric HImH<sup>+</sup> gives rise to only a single transition. Remarkably, the spacing between the two HIm resonances in the condensed phase is significantly smaller than the value of 2.4 eV observed in the gas phase for isolated HIm.<sup>40</sup> This observation underlines the ability of X-ray absorption spectroscopy to detect changes in the local charge density and

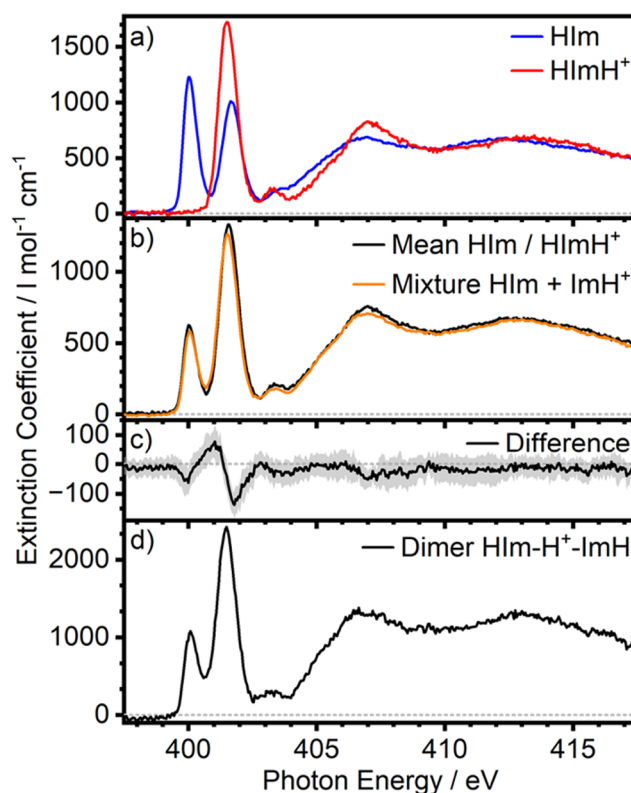


**Figure 2.** a) Nitrogen K-edge absorption spectra of HIm and HImH<sup>+</sup> at  $c = 1\text{ M}$  in ethanol. b) Spectrum of a mixture of HIm and HImH<sup>+</sup> ( $c = 0.5\text{ M}$  each) versus the arithmetic mean of the spectra for the separate components and c) the difference between them (shaded area: 68% confidence intervals). d) Spectrum derived for the HIm–H<sup>+</sup>–ImH dimer.

electric potential caused by hydrogen bond donation and acceptance via characteristic core-level shifts.

Turning now to the spectrum of the imidazole–imidazolium mixture shown in Figure 2b, deviations from the arithmetic mean of the individual spectra are observable. This becomes most evident when looking at the difference spectrum (Figure 2c), where a new feature centered at 401 eV can be found, accompanied by a reduced intensity at the peak positions of HIm and HImH<sup>+</sup>. In order to obtain a pure spectrum of the HIm–H<sup>+</sup>–ImH dimer from the recorded spectra, knowledge of the relative abundance of dimers in the investigated mixture is required. Toward this end, the equilibrium constant for the formation of the HIm–H<sup>+</sup>–ImH dimer was derived from a series of FTIR measurements as a function of sample concentration (Figure S1). We infer that a fraction of roughly 40% of the imidazole molecules forms HIm–H<sup>+</sup>–ImH dimers at the concentrations employed in the soft X-ray study ( $c(\text{HIm}) = c(\text{HImH}^+) = 0.5\text{ M}$ ). Accordingly, we derived the pure dimer spectrum in Figure 2d from the measured spectrum of the mixture by subtracting a 60% contribution of the monomer spectra. The main characteristic of the obtained spectrum is an increased absorption strength in between the two  $N_{1s} \rightarrow \pi^*$  transitions, accompanied by a slight shift of the former N lone pair peak to higher photon energies by 50 meV, while the position of the second peak matches well with the value found for the N–H side in HImH<sup>+</sup> at 401.5 eV.

The same experiment was also performed in water as solvent and yielded a similar new absorption resonance right between

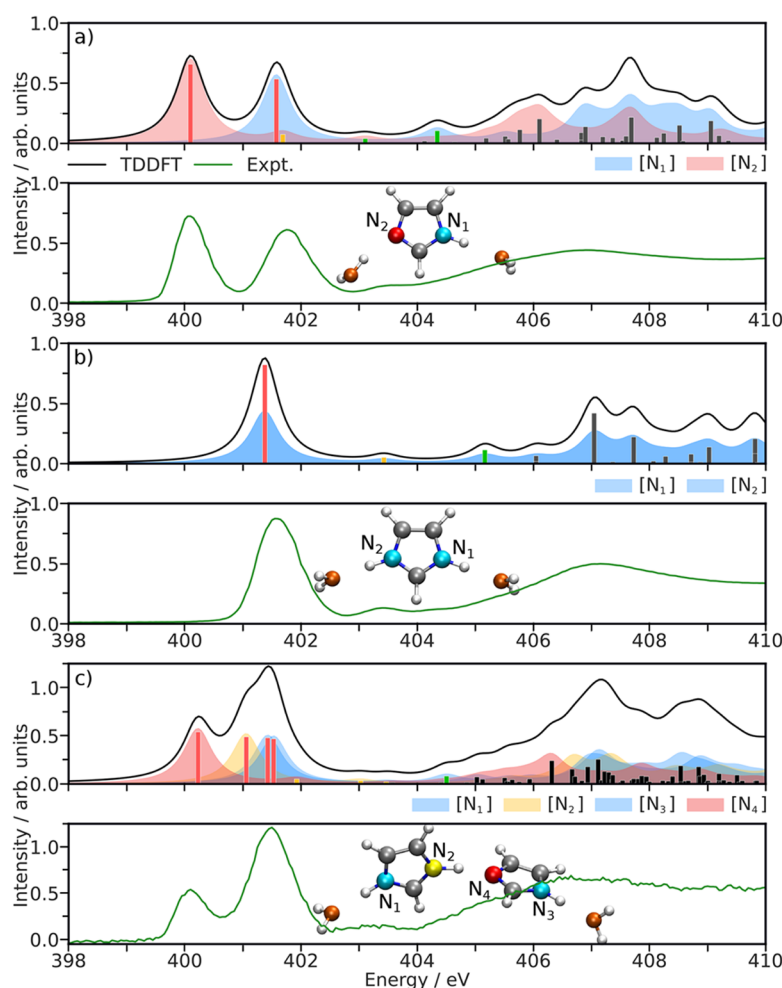


**Figure 3.** Computed XA spectra for a) HIm, b) HImH<sup>+</sup>, and c) the HIm-H<sup>+</sup>-ImH complex in aqueous solution. Contributions of the individual N sites to the spectra (black) are color-coded. Experimental data (green) were measured in water (monomers) and ethanol (HIm-H<sup>+</sup>-ImH dimer). Solid bars mark the orbital character of excitations: red ( $\pi_1^*$ ), yellow ( $\pi_2^*$ ), green ( $\sigma^*$ ), and black (other).

the known HIm and HImH<sup>+</sup> absorption features, albeit with a lower magnitude (Figure S4). This can be rationalized by the higher self-concentration of water (55.3 M) compared to that of ethanol (17.1 M) and its higher polarity as a solvent, both of which lead to a stronger solvation of the monomers<sup>56</sup> and a lower proportion of HIm-H<sup>+</sup>-ImH dimers.

With the objective to explore how the sharing of the excess proton in the HIm-H<sup>+</sup>-ImH dimer is reflected in the core excitations at the chemically distinct nitrogen sites, we simulated nitrogen K-edge spectra using time-dependent density functional theory (TDDFT) in the ORCA-5.0.3 suite of programs.<sup>46,57–60</sup> Various geometries, including the asymmetric and symmetric dimer structure with or without implicit solvation by water or ethanol, have been tested (Figure S7). In general, our analysis did not reveal any relevant change to the calculated spectral features when the polar solvent was switched from ethanol to water (Figure S8). Thus, in all further theoretical investigations presented, water was used as the solvent. Lists of tabulated excitation energies can be found in the Supporting Information (Tables S2 and S3).

The calculated spectra are shown in Figure 3 and are highly consistent with the experimental results, as they correctly reproduce all of the main pre-edge features. As discussed in the Supporting Information, a constant energy shift of 12.238 eV is

applied to all TDDFT transitions for alignment with the experimental data. First, the monomer spectrum of HIm can be disentangled into the contributions of its two nitrogen sides, with the lower-energy pre-edge peak originating from N<sub>2</sub> with the electron lone pair and the higher-energy core excitation being assigned to N<sub>1</sub> in the N–H group. On the other hand, the single intense peak in the pre-edge region of the HImH<sup>+</sup> spectrum results from core excitations at the two, in this case, equivalent nitrogen centers. Besides the characteristic large core-level shift that accompanies protonation at the N<sub>2</sub> side, the excitation energy at the N–H bonded N<sub>1</sub> side is also affected and moves to lower photon energies (exp.: 0.25 eV/calc.: 0.20 eV). Confirming the viability of our solvation model, our simulations successfully account for the solvent-induced narrowing in the separation of the pre-edge resonances in HIm compared to the gas phase, which was also observed experimentally (exp.: 1.65 eV/calc.: 1.48 eV).<sup>41</sup>

On turning to the HIm-H<sup>+</sup>-ImH dimer, the experimental spectrum in the lower panel exhibits two strong peaks on the pre-edge, the second of which is almost 2 times higher than the first. There is also significant intensity in the region in between both resonances. As we spectrally break down the computed spectrum for the asymmetric HIm-H<sup>+</sup>-ImH model in Figure 3c, the second resonance is found to originate from core

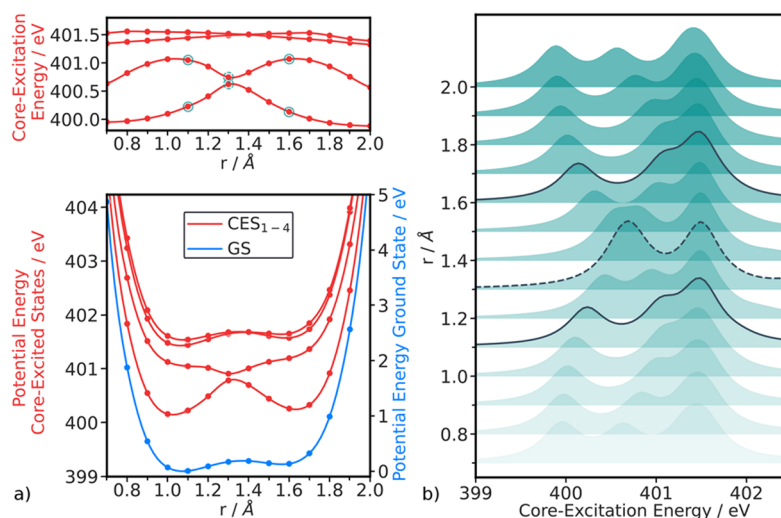


**Figure 4.** a) Bottom: ground-state potential (blue) and core excited states' energies (red) of the  $\text{Asymm}^{\text{sol}}$  complex along the proton displacement coordinate  $r$ . Top: first four core excitation energies. b) Derived XA spectra for various positions of  $r$ . Entries that belong to particularly prominent structures are highlighted by black lines and open circles.

excitations of three different nitrogen atoms. The major contribution stems from the  $\text{N}_1$  and  $\text{N}_3$  sites forming the outer two N–H groups, which act as hydrogen bond donating centers to the surrounding solvent. Energetically, the two associated transitions shown by the blue shaded areas are barely separated at 401.43 and 401.53 eV and fall right in between the calculated transition energies of the N–H group in HIm (401.58 eV) and  $\text{HImH}^+$  (401.38 eV). By contrast, nitrogen centers  $\text{N}_2$  and  $\text{N}_4$  sharing the excess proton in the dimer exhibit more distinct spectral signatures.  $\text{N}_4$  is responsible for the lowest-energy resonance at 400.23 eV (red shaded area), coming close to the value of 400.1 eV for the N lone pair side in HIm. Finally, the contribution of the  $\text{N}_2$  side, which is the one with the shorter N–H distance in the asymmetric dimer, is intermediate in energy at 401.06 eV (yellow-shaded area) and appears as a shoulder to the resonances of the outer N–H groups in the calculated N K-edge spectrum. Overall, the spectral simulations for the asymmetric dimer paint the anticipated picture of a more localized proton in which the inner nitrogen on one ring largely retains its imidazole-like character while the hydrogen bond on the other inner nitrogen is weakened compared to  $\text{HImH}^+$ , leading to a significant red shift in core excitation energy.

In our analysis, we have also assigned orbital character to the major core-to-valence transitions in terms of both canonical and natural transition orbitals (NTO).<sup>61,62</sup> In doing so, we go beyond a previous combined X-ray fluorescence and theoretical study of the HIm and  $\text{HImH}^+$  monomers.<sup>42</sup> We find that the first three excitations from each N center ( $\text{N}_1$  and  $\text{N}_2$ ) in the imidazole sample solutions correspond to equivalent core excitations to valence orbitals with  $\pi_1^*$ ,  $\pi_2^*$ , and  $\sigma^*$  character in the HIm and  $\text{HImH}^+$  moieties. The transitions in the dimer species follow the equivalent core excitations of its constituting monomers, where the four dominant features of the pre-edge all have  $\text{N}_{1s} \rightarrow \pi_1^*$  character, as displayed in Figures S9 and S10.

Considering that the spectral simulations at the global minimum in the asymmetric dimer can provide insight into the experimental reality only from the perspective of one particular

limiting case, we computed soft X-ray spectra as a function of the central N–H distance. Toward that end, we calculated the potential energy surfaces of the ground state and lowest core excited states for a rigid one-dimensional scan along the proton displacement coordinate  $r$  in the  $\text{HIm-H}^+\text{-HIm}$  complex, basically mimicking the motion of the shared proton in an asymmetric potential between the two inner nitrogen atoms. Shown in Figure 4a (bottom) are the energy profiles of the first four core excited states  $\text{CES}_{1-4}$ , which are representative of the pre-edge features in the X-ray absorption spectrum of the  $\text{HIm-H}^+\text{-ImH}$  complex and correspond to the  $\text{N}_{1s} \rightarrow \pi_1^*$  excitations from the four chemically distinguishable nitrogen sides. Notably, the PESs of  $\text{CES}_1$  and  $\text{CES}_2$  associated with the excitations on the two inner nitrogen atoms exhibit vastly different shapes and are well separated at both minima of the ground-state PES. As the shared proton approaches the barrier, the energy difference between them gradually decreases. Ultimately, at the one-dimensional saddle point, the states become nearly degenerate. On the contrary,  $\text{CES}_3$  and  $\text{CES}_4$ , originating from excitations at the outer two nitrogen atoms of the dimer, remain nearly degenerate along  $r$  and are similar in shape to the ground-state potential. This entails immediate consequences for the respective excitation energies plotted in Figure 4a (top) and for the N–K edge spectra derived at selected locations of the shared proton (Figure 4b). Because of their similarity, the curves of core excitation energies for  $\text{CES}_3$  and  $\text{CES}_4$  are almost identical and virtually flat, resulting in a single peak at a constant energy of about 401.5 eV in the X-ray spectra. Essentially, the two outer nitrogen atoms in the N–H groups act more like local spectators and are not very sensitive to the whereabouts of the shared proton. Most of the details about the electronic structure of the LBHB complex lie in the spectral X-ray signatures of  $\text{CES}_1$  and  $\text{CES}_2$  directly probing the hydrogen-bonded inner nitrogen atoms. In the global minimum geometry of the asymmetric dimer (solid black line,  $r = 1.1 \text{ \AA}$ ), the lowest-energy peak can be assigned to  $\text{CES}_1$  and corresponds to the core excitation on the “lone pair” nitrogen side  $\text{N}_4$  whereas the intermediate feature originates from  $\text{CES}_2$  (i.e., the nitrogen side  $\text{N}_2$  where the shared proton is closer). Upon movement of the proton along the  $\text{N}\cdots\text{H}\cdots\text{N}$  axis toward

the central barrier, the core excitation energies and thus also the two peaks in the X-ray spectrum converge.  $\text{CES}_1$  shifts to higher energies as the  $\text{N}_4$  side partially loses its imidazole character due to the proton getting closer and vice versa for  $\text{CES}_2$  and the  $\text{N}_2$  side. At  $r = 1.3 \text{ \AA}$  (dashed line), the proton is located exactly in the middle of the two inner nitrogen atoms which become virtually identical from an X-ray spectroscopic perspective. Evidently, an evenly shared proton generates a spectrum with only two pre-edge transitions originating from the two doubly degenerate core-level excitations at the inner and outer nitrogen sides, respectively. A further movement of the proton to the second, local minimum of the double potential at  $1.6 \text{ \AA}$  results in a spectrum which resembles the one obtained in the global minimum. However, since the sides for the shared proton in the HIm- $\text{H}^+$ -ImH dimer have been switched, the low-energy  $\text{CES}_1$  is now localized at  $\text{N}_2$  while  $\text{CES}_2$  now belongs to  $\text{N}_4$ .

For comparison, we also computed the PES for the core excited states in the symmetrically optimized dimer geometry (Figure S11). We find that the core excitations acquired along the proton-transfer coordinate are barely affected by the overall geometry of the complex, mostly because the ground and core excited states exhibit similar (a)symmetries which in all cases lead to a quite equivalent progression of core excitation energies and thus pre-edge peak positions. Deviations thereof are mainly observable in the direct vicinity of the saddle point of the central barrier in the asymmetric dimer.

Having benchmarked the sensitivity of soft X-ray spectroscopy with respect to the exact positioning of the shared proton in the double-minimum potential of the HIm- $\text{H}^+$ -ImH dimer, it is further necessary to consider the relative contributions of the various calculated spectra to the overall experimental result. While a complete quantum dynamical description of the nuclear wave function over a freely relaxed potential would be desirable, this is beyond the scope of the current study. Instead, with an estimation based on a numerical solution,<sup>63,64</sup> we assessed the ground-state vibrational eigenfunction for the central proton based on the symmetric and asymmetric ground-state potentials, respectively (Figure 5a). The more localized nature of the shared proton in the asymmetric case is clearly reflected by the shape of the respective eigenfunction, while the highest likeliness to locate the proton in the symmetric case is right in between the two central nitrogen atoms. To include this degree of localization and delocalization, we have computed weighted X-ray absorption spectra based on the density of the eigenfunctions. Each absorption spectrum from Figure 4b is scaled according to its corresponding contribution from the ground-state nuclear eigenfunction and finally summed to generate an overall spectrum for both the asymmetric and symmetric dimer geometries. Results of this procedure are shown in Figure 5b and compared to the single spectrum where the proton is located in the global minimum of the asymmetric dimer. For the asymmetric case, the analysis demonstrates that the shape of the pre-edge features does not undergo significant changes when the entire weighted distribution of the spectra is taken into account instead of considering only the spectrum at the global minimum. On the other hand, the spectrum in the symmetric potential has a major contribution from core excitations near the saddle point of the double-minimum potential. In accordance with Figure 4b, this results in a single broad peak which originates from the core excitations at both

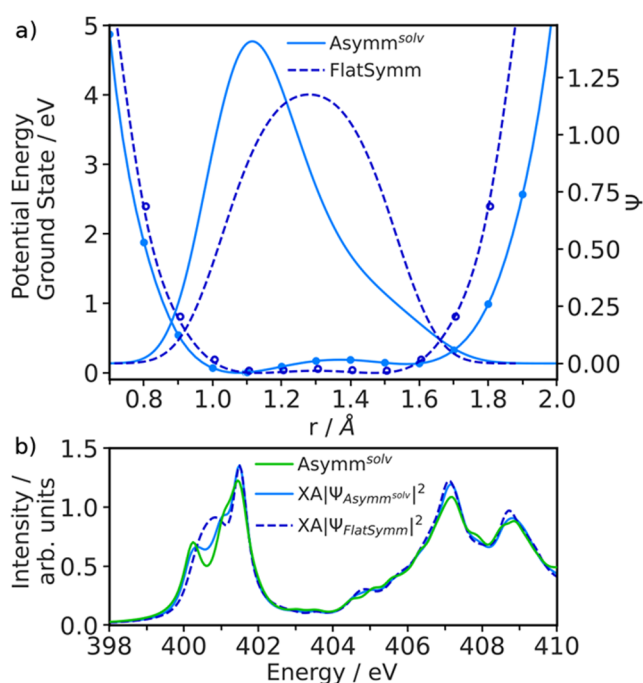


**Figure 5.** a) Ground-state potentials of the asymmetric ( $\text{Asymm}^{\text{solv}}$ ) and symmetric ( $\text{FlatSymm}$ ) complex along the proton displacement coordinate  $r$  and their corresponding nuclear eigenfunctions. b) XA spectra calculated by weighting the distribution of spectra (Figure 4b) by the amplitude of the eigenfunction in the asymmetric potential (blue) and symmetric potential (dashed blue). For comparison, XA spectrum at the minimum of the asymmetric structure (green).

of the inner nitrogen atoms, as a signature of the delocalized nature of the equally shared proton.

Ultimately, in comparison to the measurement results, it has to be taken into consideration that the theoretically distinguishable level of detail is beyond reach experimentally, not only for reasons of energy resolution but also because of the proportion of complex formation and flat jet operating stability at high molar concentrations. What can be inferred from the experimental data, however, is that the spectrum of the dimer retains the substantial character of the HIm and HIm $\text{H}^+$  monomers. The more subtle difference lies in an increased absorption cross section halfway between those of the  $\text{N}_{1s} \rightarrow \pi^*$  transitions indicative of the imidazole monomer N lone pair and N–H functionalities. This would render the scenario of a fully delocalized shared proton less likely, as the HIm spectral signature is partially lost in the symmetric structure, while a description that implies a certain degree of localization leads to higher agreement between experiment and theory (Figure 5b and Figure S12).

In summary, we show with this study how nitrogen core excitations can be used to grasp the impact of the proton on the electronic structure of protonated imidazole dimers, where the proton is shared by two imidazole units in a superstrong low-barrier hydrogen bond. As a main spectroscopic finding, we identify an increased absorbance right in between the known nitrogen K-edge transitions of pure imidazole and imidazolium. DFT-based spectral calculations confirm the assignment of the new feature as an electronic fingerprint of the proton in a double-well potential. Instead of interrogating the proton directly, we observe that the chemically distinct nitrogen sites involved in the hydrogen bonding show a strong dependence on the double-well potential energy of the proton-

transfer mode. An asymmetric proton sharing potential with a higher barrier for proton transfer results in a rather localized proton with X-ray signatures reminiscent of the monomers. On the other hand, with an increasingly symmetrical potential, the spectroscopic characteristics of the internal nitrogen compounds become more similar and finally are indistinguishable in the state of a low-barrier superstrong hydrogen bond with a fully delocalized proton. Proceeding from the two-case scenario presented here, where the central N...N distance is found to dictate the shape of the potential energy landscape for the shared proton, further simulations could consider a wider variety of geometries occurring in the fluctuating solvent environment and incorporate the role of quantum phenomena such as proton tunneling. Future exploration of the ultrafast transient response of these nitrogen K-edge transitions would lead to valuable information on the nature of the electronic structural dynamics of the protonated imidazole dimer, be it through inner hydrogen bond modulation of the two imidazole units or the impact of the fluctuating solvent electrical field on the positively charged inner proton.

## ■ ASSOCIATED CONTENT

### SI Supporting Information

The Supporting Information is available free of charge at <https://pubs.acs.org/doi/10.1021/acs.jpcllett.3c03576>.

Experimental and computational details, FTIR and XA spectra, calculated molecular structures, orbital assignment to transitions, NTO analysis, tabulated core excitation energies, and nuclear wave function calculations (PDF)

## ■ AUTHOR INFORMATION

### Corresponding Authors

**Sambit K. Das** – Department of Physics, Stockholm University, AlbaNova University Center, SE-106 91 Stockholm, Sweden; Email: [sambit.das@fysik.su.se](mailto:sambit.das@fysik.su.se)

**Marc-Oliver Winghart** – Max Born Institut für Nichtlineare Optik und Kurzzeitspektroskopie, 12489 Berlin, Germany; [orcid.org/0009-0003-0213-4010](https://orcid.org/0009-0003-0213-4010); Email: [winghart@mbi-berlin.de](mailto:winghart@mbi-berlin.de)

**Erik T. J. Nibbering** – Max Born Institut für Nichtlineare Optik und Kurzzeitspektroskopie, 12489 Berlin, Germany; [orcid.org/0000-0001-5874-8052](https://orcid.org/0000-0001-5874-8052); Email: [nibberin@mbi-berlin.de](mailto:nibberin@mbi-berlin.de)

**Michael Odellius** – Department of Physics, Stockholm University, AlbaNova University Center, SE-106 91 Stockholm, Sweden; [orcid.org/0000-0002-7023-2486](https://orcid.org/0000-0002-7023-2486); Email: [odellius@fysik.su.se](mailto:odellius@fysik.su.se)

### Authors

**Peng Han** – Max Born Institut für Nichtlineare Optik und Kurzzeitspektroskopie, 12489 Berlin, Germany

**Debkumar Rana** – Max Born Institut für Nichtlineare Optik und Kurzzeitspektroskopie, 12489 Berlin, Germany; [orcid.org/0000-0001-8165-3289](https://orcid.org/0000-0001-8165-3289)

**Zhuang-Yan Zhang** – Max Born Institut für Nichtlineare Optik und Kurzzeitspektroskopie, 12489 Berlin, Germany

**Sebastian Eckert** – Institute for Methods and Instrumentation for Synchrotron Radiation Research, Helmholtz-Zentrum Berlin für Materialien und Energie GmbH, 12489 Berlin, Germany; [orcid.org/0000-0002-1310-0735](https://orcid.org/0000-0002-1310-0735)

**Mattis Fondell** – Institute for Methods and Instrumentation for Synchrotron Radiation Research, Helmholtz-Zentrum Berlin für Materialien und Energie GmbH, 12489 Berlin, Germany

**Thomas Schnappinger** – Department of Physics, Stockholm University, AlbaNova University Center, SE-106 91 Stockholm, Sweden; [orcid.org/0000-0003-4538-811X](https://orcid.org/0000-0003-4538-811X)

Complete contact information is available at: <https://pubs.acs.org/10.1021/acs.jpcllett.3c03576>

### Author Contributions

<sup>§</sup>S.K.D. and M.-O.W. contributed equally to this work

### Notes

The authors declare no competing financial interest.

## ■ ACKNOWLEDGMENTS

S.K.D. and M.O. acknowledge funding from Swedish Research Council grant agreement no. 2021-04521 and the European Union's Horizon 2020 Research and Innovation Programme under Marie Skłodowska-Curie grant agreement no. 860553 (ITN Network SMART-X). The computations were enabled by resources provided by the National Academic Infrastructure for Supercomputing in Sweden (NAISS) and the Swedish National Infrastructure for Computing (SNIC) at NSC and PDC partially funded by the Swedish Research Council through grant agreement no. 2022-06725 and no. 2018-05973. M.-O.W., P.H., D.R., Z.-Y.Z., and E.T.J.N. cordially acknowledge the financial support from the European Research Council (ERC) under the European Union's Horizon 2020 Research and Innovation Programme (ERC grant agreement no. 788704, E.T.J.N.) and the ITN Network SMART-X. We all greatly acknowledge the support of the BESSYII staff during X-ray measurements at the variable polarization undulator beamline UE52\_SGM of the Helmholtz-Zentrum Berlin, and we thank Helmholtz-Zentrum Berlin for the allocation of synchrotron radiation beam time.

## ■ REFERENCES

- (1) Gilli, G.; Gilli, P. *The Nature of the Hydrogen Bond: Outline of a Comprehensive Hydrogen Bond Theory*; Oxford University Press: New York, 2009.
- (2) Novak, A. Hydrogen Bonding in Solids. Correlation of Spectroscopic and Crystallographic Data. *Struct. Bonding (Berlin)* **1974**, *18*, 177–216.
- (3) Mikenda, W. Stretching Frequency versus Bond Distance Correlation of O-D(H)...Y (Y = N, O, S, Se, Cl, Br, I) Hydrogen Bonds in Solid Hydrates. *J. Mol. Struct.* **1986**, *147*, 1–15.
- (4) Lantié, A.; Froment, F.; Novak, A. Relationship Between NH Stretching Frequencies and N...O Distances of Crystals Containing NH...O Hydrogen Bonds. *Spectrosc. Lett.* **1976**, *9*, 289–299.
- (5) Hadži, D.; Bratos, S. In *The Hydrogen Bond: Recent Developments in Theory and Experiments*; Schuster, P., Zundel, G., Sandorfy, C., Eds.; North-Holland: Amsterdam, 1976.
- (6) Schiøtt, B.; Iversen, B. B.; Madsen, G. K. H.; Larsen, F. K.; Bruice, T. C. On the Electronic Nature of Low-Barrier Hydrogen Bonds in Enzymatic Reactions. *Proc. Natl. Acad. Sci. U.S.A.* **1998**, *95*, 12799–12802.
- (7) Warshel, A.; Sharma, P. K.; Kato, M.; Xiang, Y.; Liu, H.; Olsson, M. H. M. Electrostatic Basis for Enzyme Catalysis. *Chem. Rev.* **2006**, *106*, 3210–3235.
- (8) Kreuer, K. On the Complexity of Proton Conduction Phenomena. *Solid State Ionics* **2000**, 136–137, 149–160.
- (9) Kreuer, K.-D.; Paddison, S. J.; Spohr, E.; Schuster, M. Transport in Proton Conductors for Fuel-Cell Applications: Simulations,

Elementary Reactions, and Phenomenology. *Chem. Rev.* **2004**, *104*, 4637–4678.

(10) Kreuer, K.-D.; Münchinger, A. Fast and Selective Ionic Transport: From Ion-Conducting Channels to Ion Exchange Membranes for Flow Batteries. *Annu. Rev. Mater. Res.* **2021**, *51*, 21–46.

(11) Zundel, G.; Metzger, H. Energiebänder Der Tunnelnden Überschuss-Protonen in Flüssigen Säuren. Eine IR-spektroskopische Untersuchung Der Natur Der Gruppierungen  $H_5O_2^+$ . *Z. Phys. Chem.* **1968**, *58*, 225–245.

(12) Zundel, G. Hydrogen Bonds with Large Proton Polarizability and Proton Transfer Processes in Electrochemistry and Biology. *Adv. Chem. Phys.* **1999**, *111*, 1–217.

(13) Olesen, S.; Guasco, T.; Roscioli, J.; Johnson, M. Tuning the Intermolecular Proton Bond in the  $H_5O_2^+$  ‘Zundel Ion’ Scaffold. *Chem. Phys. Lett.* **2011**, *509*, 89–95.

(14) Eigen, M. Proton Transfer, Acid-Base Catalysis, and Enzymatic Hydrolysis. Part I: Elementary Processes. *Angew. Chem., Int. Ed.* **1964**, *3*, 1–19.

(15) Meiboom, S. Nuclear Magnetic Resonance Study of the Proton Transfer in Water. *J. Chem. Phys.* **1961**, *34*, 375–388.

(16) Dahms, F.; Costard, R.; Pines, E.; Fingerhut, B. P.; Nibbering, E. T. J.; Elsaesser, T. The Hydrated Excess Proton in the Zundel Cation  $H_5O_2^+$ : The Role of Ultrafast Solvent Fluctuations. *Angew. Chem., Int. Ed.* **2016**, *55*, 10600–10605.

(17) Fournier, J. A.; Carpenter, W. B.; Lewis, N. H. C.; Tokmakoff, A. Broadband 2D IR Spectroscopy Reveals Dominant Asymmetric  $H_5O_2^+$  Proton Hydration Structures in Acid Solutions. *Nat. Chemistry* **2018**, *10*, 932–937.

(18) Dereka, B.; Yu, Q.; Lewis, N. H. C.; Carpenter, W. B.; Bowman, J. M.; Tokmakoff, A. Crossover from Hydrogen to Chemical Bonding. *Science* **2021**, *371*, 160–164.

(19) Marx, D.; Tuckerman, M. E.; Hutter, J.; Parrinello, M. The Nature of the Hydrated Excess Proton in Water. *Nature* **1999**, *397*, 601–604.

(20) Vuilleumier, R.; Borgis, D. Transport and Spectroscopy of the Hydrated Proton: A Molecular Dynamics Study. *J. Chem. Phys.* **1999**, *111*, 4251–4266.

(21) Schmitt, U. W.; Voth, G. A. The Computer Simulation of Proton Transport in Water. *J. Chem. Phys.* **1999**, *111*, 9361–9381.

(22) Kirchner, B. Eigen or Zundel Ion: News from Calculated and Experimental Photoelectron Spectroscopy. *ChemPhysChem* **2007**, *8*, 41–43.

(23) Gasparotto, P.; Hassanali, A. A.; Ceriotti, M. Probing Defects and Correlations in the Hydrogen-bond Network of ab initio Water. *J. Chem. Theory Comput.* **2016**, *12*, 1953–1964.

(24) Marx, D. Proton Transfer 200 Years After Von Grotthuss: Insights from ab initio Simulations. *ChemPhysChem* **2006**, *7*, 1848–1870.

(25) Tuckerman, M. E.; Marx, D.; Klein, M. L.; Parrinello, M. On the Quantum Nature of the Shared Proton in Hydrogen Bonds. *Science* **1997**, *275*, 817–820.

(26) Cavalleri, M.; Näslund, L.-Å.; Edwards, D. C.; Wernet, P.; Ogasawara, H.; Myneni, S.; Ojamäe, L.; Odelius, M.; Nilsson, A.; Pettersson, L. G. M. The Local Structure of Protonated Water from X-Ray Absorption and Density Functional Theory. *J. Chem. Phys.* **2006**, *124*, 194508.

(27) Cappa, C. D.; Smith, J. D.; Messer, B. M.; Cohen, R. C.; Saykally, R. J. The Electronic Structure of the Hydrated Proton: A Comparative X-ray Absorption Study of Aqueous HCl and NaCl Solutions. *J. Phys. Chem. B* **2006**, *110*, 1166–1171.

(28) Margarella, A. M.; Perrine, K. A.; Lewis, T.; Faubel, M.; Winter, B.; Hemminger, J. C. Dissociation of Sulfuric Acid in Aqueous Solution: Determination of the Photoelectron Spectral Fingerprints of  $H_2SO_4$ ,  $HSO_4^-$ , and  $SO_4^{2-}$  in Water. *J. Phys. Chem. C* **2013**, *117*, 8131–8137.

(29) Ekimova, M.; Kleine, C.; Ludwig, J.; Ochmann, M.; Agrenius, T. E. G.; Kozari, E.; Pines, D.; Pines, E.; Huse, N.; Wernet, P.; et al. From Local Covalent Bonding to Extended Electric Field Interactions

in Proton Hydration. *Angew. Chem., Int. Ed.* **2022**, *61*, No. e202211066.

(30) Münch, W.; Kreuer, K.-D.; Silvestri, W.; Maier, J.; Seifert, G. The Diffusion Mechanism of an Excess Proton in Imidazole Molecule Chains: First Results of an Ab Initio Molecular Dynamics Study. *Solid State Ionics* **2001**, *145*, 437–443.

(31) Schuster, M.; Meyer, W.; Wegner, G.; Herz, H.; Ise, M.; Schuster, M.; Kreuer, K.; Maier, J. Proton Mobility in Oligomer-Bound Proton Solvents: Imidazole Immobilization via Flexible Spacers. *Solid State Ionics* **2001**, *145*, 85–92.

(32) Scharfenberger, G.; Meyer, W. H.; Wegner, G.; Schuster, M.; Kreuer, K.-D.; Maier, J. Anhydrous Polymeric Proton Conductors Based on Imidazole Functionalized Polysiloxane. *Fuel Cells* **2006**, *6*, 237–250.

(33) Chen, H.; Yan, T.; Voth, G. A. A Computer Simulation Model for Proton Transport in Liquid Imidazole. *J. Phys. Chem. A* **2009**, *113*, 4507–4517.

(34) Long, Z.; Atsango, A. O.; Napoli, J. A.; Markland, T. E.; Tuckerman, M. E. Elucidating the Proton Transport Pathways in Liquid Imidazole with First-Principles Molecular Dynamics. *J. Phys. Chem. Lett.* **2020**, *11*, 6156–6163.

(35) Melchior, J.-P.; Majer, G.; Kreuer, K.-D. Why Do Proton Conducting Polybenzimidazole Phosphoric Acid Membranes Perform Well in High-Temperature PEM Fuel Cells? *Phys. Chem. Chem. Phys.* **2017**, *19*, 601–612.

(36) Blow, D. M.; Birktoft, J. J.; Hartley, B. S. Role of a Buried Acid Group in the Mechanism of Action of Chymotrypsin. *Nature* **1969**, *221*, 337–340.

(37) Kumar, P.; Agarwal, P. K.; Cuneo, M. J. On the Case of the Misplaced Hydrogens. *ChemBioChem* **2021**, *22*, 288–297.

(38) Gerlt, J. A.; Kreevoy, M. M.; Cleland, W.; Frey, P. A. Understanding Enzymic Catalysis: The Importance of Short, Strong Hydrogen Bonds. *Chem. Biol.* **1997**, *4*, 259–267.

(39) Decoursey, T. E. Voltage-Gated Proton Channels and Other Proton Transfer Pathways. *Physiol. Rev.* **2003**, *83*, 475–579.

(40) Apen, E.; Hitchcock, A. P.; Gland, J. L. Experimental Studies of the Core Excitation of Imidazole, 4,5-Dicyanoimidazole, and s-Triazine. *J. Phys. Chem.* **1993**, *97*, 6859–6866.

(41) Thomason, M. J.; Seabourne, C. R.; Sattelle, B. M.; Hembury, G. A.; Stevens, J. S.; Scott, A. J.; Aziz, E. F.; Schroeder, S. L. M. Self-Association of Organic Solutes in Solution: A NEXAFS Study of Aqueous Imidazole. *Faraday Discuss.* **2015**, *179*, 269–289.

(42) Meyer, F.; Blum, M.; Benkert, A.; Hauschild, D.; Jeyachandran, Y. L.; Wilks, R. G.; Yang, W.; Bär, M.; Reinert, F.; Heske, C.; et al. Site-Specific Electronic Structure of Imidazole and Imidazolium in Aqueous Solutions. *Phys. Chem. Chem. Phys.* **2018**, *20*, 8302–8310.

(43) Dahms, F.; Fingerhut, B. P.; Nibbering, E. T. J.; Pines, E.; Elsaesser, T. Large-Amplitude Transfer Motion of Hydrated Excess Protons Mapped by Ultrafast 2D IR Spectroscopy. *Science* **2017**, *357*, 491–495.

(44) Frisch, M. J.; Trucks, G. W.; Schlegel, H. B.; Scuseria, G. E.; Robb, M. A.; Cheeseman, J. R.; Scalmani, G.; Barone, V.; Petersson, G. A.; Nakatsuji, H. et al. *Gaussian 16*, Revision C.01; Gaussian Inc.: Wallingford, CT, 2016.

(45) Chai, J.-D.; Head-Gordon, M. Long-Range Corrected Hybrid Density Functionals with Damped Atom–Atom Dispersion Corrections. *Phys. Chem. Chem. Phys.* **2008**, *10*, 6615–6620.

(46) Weigend, F.; Ahlrichs, R. Balanced Basis Sets of Split Valence, Triple Zeta Valence and Quadruple Zeta Valence Quality for H to Rn: Design and Assessment of Accuracy. *Phys. Chem. Chem. Phys.* **2005**, *7*, 3297–3305.

(47) Tatara, W.; Wójcik, M. J.; Lindgren, J.; Probst, M. Theoretical Study of Structures, Energies, and Vibrational Spectra of the Imidazole-Imidazolium System. *J. Phys. Chem. A* **2003**, *107*, 7827–7831.

(48) Gerardi, H. K.; Gardenier, G. H.; Viswanathan, U.; Auerbach, S. M.; Johnson, M. A. Vibrational Predissociation Spectroscopy and Theory of Ar-tagged, Protonated Imidazole (Im)  $Im_{1-3}H^+$ -Ar Clusters. *Chem. Phys. Lett.* **2011**, *501*, 172–178.

(49) Tikhonov, D. S.; Scutelnic, V.; Sharapa, D. I.; Krotova, A. A.; Dmitrieva, A. V.; Obenchain, D. A.; Schnell, M. Structures of the (Imidazole)<sub>n</sub>H<sup>+</sup> ...Ar (N = 1,2,3) Complexes Determined from IR Spectroscopy and Quantum Chemical Calculations. *Struct. Chem.* **2023**, *34*, 203–213.

(50) Ekimova, M.; Quevedo, W.; Szyk, Ł.; Iannuzzi, M.; Wernet, P.; Odelius, M.; Nibbering, E. T. Aqueous Solvation of Ammonia and Ammonium: Probing Hydrogen Bond Motifs with FT-IR and Soft X-ray Spectroscopy. *J. Am. Chem. Soc.* **2017**, *139*, 12773–12783.

(51) Ekimova, M.; Kubin, M.; Ochmann, M.; Ludwig, J.; Huse, N.; Wernet, P.; Odelius, M.; Nibbering, E. T. Soft X-ray Spectroscopy of the Amine Group: Hydrogen Bond Motifs in Alkylamine/Alkylammonium Acid–Base Pairs. *J. Phys. Chem. B* **2018**, *122*, 7737–7746.

(52) Ekimova, M.; Quevedo, W.; Faubel, M.; Wernet, P.; Nibbering, E. T. J. A Liquid Flatjet System for Solution Phase Soft-x-Ray Spectroscopy. *Struct. Dyn.* **2015**, *2*, 054301.

(53) Miedema, P. S.; Quevedo, W.; Fondell, M. The Variable Polarization Undulator Beamline UES2 SGM at BESSY II. *JLSRF* **2016**, *2*, A70.

(54) Fondell, M.; Eckert, S.; Jay, R. M.; Weniger, C.; Quevedo, W.; Niskanen, J.; Kennedy, B.; Sorgenfrei, F.; Schick, D.; Giangrisostomi, E.; et al. Time-Resolved Soft X-ray Absorption Spectroscopy in Transmission Mode on Liquids at MHz Repetition Rates. *Struct. Dyn.* **2017**, *4*, 054902.

(55) Henke, B.; Gullikson, E.; Davis, J. X-Ray Interactions: Photoabsorption, Scattering, Transmission, and Reflection at E = 50–30,000 eV, Z = 1–92. *At. Data Nucl. Data Tables* **1993**, *54*, 181–342.

(56) Al-Madhagi, L. H.; Callear, S. K.; Schroeder, S. L. M. Hydrophilic and Hydrophobic Interactions in Concentrated Aqueous Imidazole Solutions: A Neutron Diffraction and Total X-ray Scattering Study. *Phys. Chem. Chem. Phys.* **2020**, *22*, 5105–5113.

(57) Neese, F. Software Update: The ORCA Program System—Version 5.0. *Wiley Interdiscip. Rev. Comput. Mol. Sci.* **2022**, *12*, No. e1606.

(58) Lin, Y.-S.; Li, G.-D.; Mao, S.-P.; Chai, J.-D. Long-Range Corrected Hybrid Density Functionals with Improved Dispersion Corrections. *J. Chem. Theory Comput.* **2013**, *9*, 263–272.

(59) Cammi, R.; Mennucci, B.; Tomasi, J. Fast Evaluation of Geometries and Properties of Excited Molecules in Solution: a Tamm-Dancoff Model with Application to 4-Dimethylaminobenzonitrile. *J. Phys. Chem. A* **2000**, *104*, 5631–5637.

(60) Izsák, R.; Neese, F. An Overlap Fitted Chain of Spheres Exchange Method. *J. Chem. Phys.* **2011**, *135*, 144105.

(61) Krylov, A. I. From Orbitals to Observables and Back. *J. Chem. Phys.* **2020**, *153*, 080901.

(62) Martin, R. L. Natural Transition Orbitals. *J. Chem. Phys.* **2003**, *118*, 4775–4777.

(63) Kosloff, R.; Tal-Ezer, H. A Direct Relaxation Method for Calculating Eigenfunctions and Eigenvalues of the Schrödinger Equation on a Grid. *Chem. Phys. Lett.* **1986**, *127*, 223–230.

(64) Smyth, E. S.; Parker, J. S.; Taylor, K. T. Numerical Integration of the Time-Dependent Schrödinger Equation for Laser-Driven Helium. *Comput. Phys. Commun.* **1998**, *114*, 1–14.